Physics and Chemistry of the Earth 110 (2019) 168–175

Contents lists available at ScienceDirect

Physics and Chemistry of the Earth

journal homepage: www.elsevier.com/locate/pce

Remote sensing image-based analysis of the urban heat island effect in Shenzhen, China

Weimin Wang[a], Kai Liu[a,*], Rong Tang[b], Shudong Wang[c]

[a] Shenzhen Environmental Monitoring Center, Shenzhen, China
[b] Beijing Forestry University, Beijing, China
[c] The Institute of Remote Sensing and Digital Earth, Chinese Academy of Sciences, Beijing, China

ARTICLE INFO

Keywords:
Urban heat island
Remote sensing
Heat flux
Shenzhen

ABSTRACT

The urban heat island effect is a typical urban climate phenomenon, and the formation and intensity of these phenomena are closely related to the land cover type. Based on Landsat 8 remote sensing images of Shenzhen, China, this study uses a linear spectral mixture model to extract land coverage information, and then analyzes the effects of urban land coverage on the land surface temperature (LST) and heat budget components. The results show that the LST of Shenzhen decreases gradually from northwest to southeast and that the LST of urban impervious surfaces are significantly higher than those of vegetation-covered areas with a difference of 3–4 K, thus demonstrating a significant urban heat island effect. Impervious surfaces and urban vegetation both affect the LST and heat budget components of Shenzhen. The impervious area contributes more to the surface sensible heat, while urban vegetation contributes more to the surface latent heat. The research results show that a very small area of urban green land (vegetation fraction coverage less than 4–8%) exhibits a strong capacity for heat dissipation. In the practice of urban construction, avoiding concentrated impervious areas and increasing urban green land areas represent effective methods of alleviating the urban heat island effect. This study helps to better understand the optimization of urban landscapes and alleviation of the urban heat island effect.

1. Introduction

Effective monitoring of the urban thermal environment can provide important insights into urban thermal spatial structures and urban development changes. A comfortable urban thermal environment has become an important reflection of the ecological environment of urban human settlements and represents an important supporting condition of socially sustainable development. With the continuous acceleration of urbanization, natural vegetation has been replaced by impervious land surfaces, such as cement and asphalt. The complexity of urban structures leads to changes in the main factors that control the land surface energy exchange, such as land surface albedo, emissivity and heat capacity (Rizwan et al., 2008). Moreover, the occurrence of living styles that are typically represented by high energy consumption leads to a gradual increase in gas emissions from artificial heat, which changes the pattern of the near-surface thermal radiation flux exchange and the microclimate of cities and surrounding areas (Oke, 1982). The manifestation of this pattern is a significant difference in the local climate between urban and suburban areas, i.e., the heat island effect. The urban heat island (UHI) is a unique phenomenon of urban ecosystems and represents one of the prominent characteristics of the impacts of anthropogenic activities on air temperature, and its effect on global climate warming has drawn wide attention (Arnfield, 2003; Li et al., 2018).

The development of thermal remote sensing provides a good solution to the flaw observed in conventional monitoring of urban heat islands (Pongrácz et al., 2010; Weng, 2009). Such techniques can quantitatively and effectively monitor the distribution characteristics of urban heat islands as well as the periodic and dynamic changes in urban thermal environments (Grimmond, 2007). Remote sensing has become an important approach for monitoring and studying the urban heat island effect (Voogt and Oke, 2003). Relevant studies initially attempted to use the moderate resolution imaging spectrometer (MODIS) and advanced very high resolution radiometer (AVHRR), which can describe the general distribution of land surface thermal characteristics (Imhoff et al., 2010; Schwarz et al., 2011; Tran et al., 2006). Moreover, the medium-resolution sensors of Landsat and ASTER have been widely used for studying local areas surface urban heat islands. For example, Chen et al. (2006) combined Landsat and Thematic Mapper (TM) technology to assess the land cover changes and spatiotemporal

* Corresponding author.
E-mail address: liukai_cas@yahoo.com (K. Liu).

https://doi.org/10.1016/j.pce.2019.01.002
Received 30 September 2018; Received in revised form 16 December 2018; Accepted 3 January 2019
Available online 07 January 2019

distribution characteristics of the UHI in the Pearl River Delta region under rapid urbanization (Kato and Yamaguchi, 2005). analyzed the urban heat-island effect of Nagoya, Japan, using ASTER and ETM + Data, mainly by exploring the anthropogenic heat discharge and natural heat radiation. Other related studies including the Liu et al. (2016), Liu et al. (2015), Weng et al. (2004), and Yuan and Bauer (2007).

The land-cover type plays an important role in urban environment changes. The accurate and timely extraction of land cover types is important for environmental monitoring and management. However, the interaction between land covers and thermal environmental variables is very complicated (Buyantuyev and Wu, 2010). Advanced models and techniques are required to describe this process, especially for typical urban-suburban areas. Particularly, the transition from natural land surface type to urban impervious layer can result in significant regional climate change. Urban thermal environments are considered a typical study variable by many researchers (Liu et al., 2014; Weng and Lu, 2008; Zhang et al., 2009). More accurate analyses of the effects of urban land use coverage on the distribution of urban land surface temperatures (LSTs) and the range and intensity of the urban heat island effect are helpful for understanding the mechanisms underlying the cause and evolution of urban heat islands. Using remote sensing techniques to study variations in the urban heat island phenomena among different land-cover types is important for the accurate monitoring of the urban heat island phenomenon and objective identification of the spatiotemporal changes of urban heat islands.

According to the above context, based on Landsat 8 remote sensing images of Shenzhen, this study extracts abundance information of land covers and further analyzes the effects of urban land coverage on LST and heat budget components. This study hopes to understand the effect of land cover patterns on the urban land surface thermal environment in Shenzhen, China and provide basic research support for the optimization of urban landscapes and the alleviation of the urban heat island effect. Because of the rapid urbanization and landscape transformation, Shenzhen has experienced substantial land-cover patterns changes, consequently resulting to a series of urban thermal environmental issues. Recently, Shenzhen has become one important area for the studies of environmental landscape patterns and a lot of references have focused on this region (Chen et al., 2012; Liu et al., 2017b; Peng et al., 2018).

2. Study region and data

Shenzhen is located in a coastal area of South China between 113°46′E and 114°37′E and between 2°27′N and 22°52′N. Its total continental area is 1952 km^2 (Fig. 1). The topography of Shenzhen is high in the southeast and low in the northwest. Hilly areas account for approximately 39.6% of the total urban area. The climate of Shenzhen is warm and humid and presents a southern subtropical maritime climate. The annual mean temperature is 22.4 °C, and the annual precipitation is 1948 mm.

In recent decades, Shenzhen has transitioned from a small border town to a highly urbanized regional economic center. With the rapid transformation of urban ecological land into hard urban construction land, the urban expansion of Shenzhen has nearly reached saturation at present. The high and rapid urbanization not only causes tremendous population pressure on the local area but also results in a continuous increase of impervious land surfaces and fragmentation of ecological land, thus leading to continuous intensification of the urban heat island effect.

This study uses one scene of Landsat 8 remote sensing images in September 2013. The spatial resolution is 30 m for the multispectral bands and 120 m for the thermal infrared wavebands. This study selects high-resolution images of SPOT-6 and Gaofen-1 satellites for the same period to assess the classification result accuracy.

With the aid of high resolution images SPOT-6 and Gaofen-1, we first geo-referenced Landsat 8 images to UTM coordinate system, and the rectification error would have to be limited to less than one pixel. FLAASH model was then used to carry out atmospheric correction, with which radiance could be converted to surface reflectance. Finally, each pair of Landsat 8 images covering the whole area of Shenzhen was piece together into one scene image that would be later chipped to the study region.

3. Methods

3.1. Landsat LST acquisition

This study uses the radiative transfer equation to acquire the LST (Sobrino et al., 2004). This method uses the measured atmospheric sounding data synchronized with the satellite transit time to estimate the atmospheric effect on land surface thermal radiation, then subtracts such atmospheric effects from the total thermal radiation observed by the satellite sensor to obtain the land surface radiation intensity and finally converts this thermal radiation intensity to the corresponding LST.

First, the thermal infrared radiation information is converted to a brightness temperature,

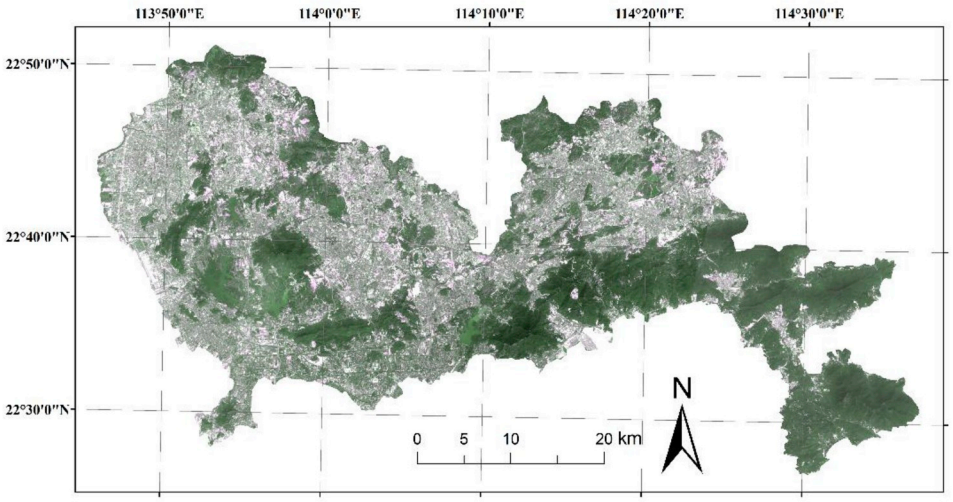

Fig. 1. True-color image of Shenzhen. (For interpretation of the references to color in this figure legend, the reader is referred to the Web version of this article.)

$$T_b = \frac{K_2}{\ln((K_1/L) + 1)} \quad (1)$$

where T_b is the brightness temperature, L is spectral radiance; K_1 and K_2 are the calibration constants.

And then, the brightness temperature can be calibrated to the LST via the surface emissivity.

$$\begin{cases} LST = \dfrac{T_b}{1 + (\lambda * T_b/\rho)\ln \varepsilon} \\ \rho = \dfrac{h * c}{\sigma} \end{cases}$$

Where λ is the wavelength of emitted radiance, σ is the Boltzmann constant, and h is the Planck's constant, C is the velocity of light.

NDVI Thresholds Method, one semi-empirical model based on urban land covers, was used in this study to obtain reliable land surface emissivity data. This method has been widely used in thermal satellite application and more descriptions can be found in Sobrino et al. (2008).

3.2. The acquisition of urban land surface heat flux

This study uses a common double-source urban heat flux model (Liu et al., 2017a; Weng et al., 2014). This heat flux model can break down the heat flux of mixed pixels into heat flux of vegetation and other non-vegetation components.

For the satellite data observed with a single angle, the vegetation and non-vegetation components of land surface within complex mixed pixels cannot be accurately separated. Therefore, the sensible heat flux H is obtained by an effective impedance method, which is as follows.

$$H = \rho C_p \frac{T_s - T_a}{VFC * R_{a\_veg} + (1 - VFC) * R_{a\_non-veg} + R_s} \quad (3)$$

where ρ is the air density, C_p is the specific heat of air at constant pressure, T_s is the surface temperature and T_a is the atmospheric temperature. R_{a_veg} and $R_{a\_non-veg}$ are the aerodynamic resistance values of vegetated and non-vegetated regions, respectively:

$$R_a = \frac{\ln\left(\frac{Z_m - d}{Z_{0m}}\right) \cdot \ln\left(\frac{Z_h - d}{Z_{0h}}\right)}{k^2 u} \quad (4)$$

where Z_m is the height of wind measurements, Z_h is the height of humidity measurements, d is the zero-plane displacement height, Z_{0m} is the roughness length governing momentum transfer, Z_{0h} is the roughness length governing transfer of heat and vapor, k is the von Karman's constant and u is the wind speed at a given height based on meteorological data.

R_s is the land surface impedance in the boundary layer, and it can be calculated using the following equation,

$$R_s = \frac{1}{a + bu_s} \quad (5)$$

where a is the free convective velocity, b is a coefficient that represents the typical soil surface roughness, and $u_s$is the wind speed over the soil surface at a height of 0.05–0.2 m.

LE can be estimated with the following equation:

$$LE = VFC * LE_{veg} + (1 - VFC) * LE_{non-veg} \quad (6)$$

where LE_{veg} and $LE_{non-veg}$are the latent heat fluxes corresponding to the vegetated and non-vegetated areas, respectively.

$$LE_{veg} = \frac{\rho C_p}{\gamma} \cdot \frac{e^o - e_a}{R_{a\_veg} + r_{s\_veg}}$$

$$LE_{non-veg} = \frac{\rho C_p}{\gamma} \cdot \frac{e^o - e_a}{R_{a\_non-veg} + r_{s\_non-veg}}$$

Where e_a is the atmospheric water vapor pressure, $e^o$is the saturation vapor pressure γ is the psychometric constant.

3.3. Classification of land covers and estimation of land coverage

This study uses the maximum likelihood classification method (Li et al., 2016; Otukei and Blaschke, 2010), in which if the observed value of a selected image sample of an unknown class is most similar to that of a sample (training) of a known class, then it is classified as that class. According to the specific characteristics of Shenzhen land use/coverage, the land cover type is divided into the following categories: urban building, cropland/grassland, tree/forest, water body and bare soil.

Most of the studies on land coverage are based on a linear spectral mixture model, which has been successfully applied to estimate land coverage from multispectral images at the subpixel scale. The decomposition of mixed pixels based on the mixture model with three or four endmembers has also achieved good results in extracting land coverage. We use the linear mixture model to calculate the components of impervious surface, vegetation, soil and shadow of each pixel of the Landsat images and compare the extracted land cover fraction with land coverage data measured on the high-resolution image. Specifically, We use a multiple endmember spectral mixture solution to extract abundance information of key urban land surfaces (Dennison and Roberts, 2003). The multiple endmember spectral mixture analysis (MESMA) allows for continuous changes of the endmember number, type and spectra to solve the problem of endmember spectral variation, thereby reducing the effects of urban landscape spatial heterogeneity on the extraction of land surface area. We select the optimal decomposition model among these models, use its endmembers as basic endmembers and consider the decomposed endmember abundance as the final abundance of the pixel. The key of the MESMA model is to determine the proper typical spectra and combination of endmembers. Considering the spectral difference of the impervious land surface, it can be divided into two endmembers with high albedo and low albedo to obtain more accurate areas of impervious layers.

4. Results analysis and discussion

4.1. Relationships between the LST, heat flux and land covers

Fig. 2 shows the land cover classification obtained from Landsat images. Fig. 3 shows the vegetation coverage results obtained from Landsat images, and Fig. 4 shows the results of impervious surfaces percentage. To evaluate the land-cover classifications accuracy, we randomly collected the validation samples from high spatial resolution images. Overall accuracy and Kappa coefficient was observed of 88.4% and 0.91, respectively, for the resulted map. Furthermore, we manually inspected and amended the classification result in latter stage. To guarantee the acceptable accuracy in percentage of impervious surfaces, regression relationship between model values and observed values was examined and an R^2 of 0.77 and a slope of 0.72 was respectively found. Moreover, a root mean square error of 8.6% and mean absolute error of 7.4% was achieved for the overall image scene, respectively.

Fig. 5 shows the results for LST derived from Landsat images. The LST map shows that the temperature of the city center is significantly higher than that of the suburban area. The area of high temperature is mainly concentrated in urban construction areas and transportation roads in the city center, including residential areas, busy commercial areas and industrial areas. These areas mainly consist of impervious materials, such as metal, asphalt and cement. In contrast, the LST corresponding to water surfaces, parks, green land and cropland are relatively low. The significant contrast between urban and suburban temperatures reveals the existence of a prominent urban heat island effect. The thermal patterns of Shenzhen exhibited in this study is basically consistent with the studies of Chen et al. (2012) and Peng et al.

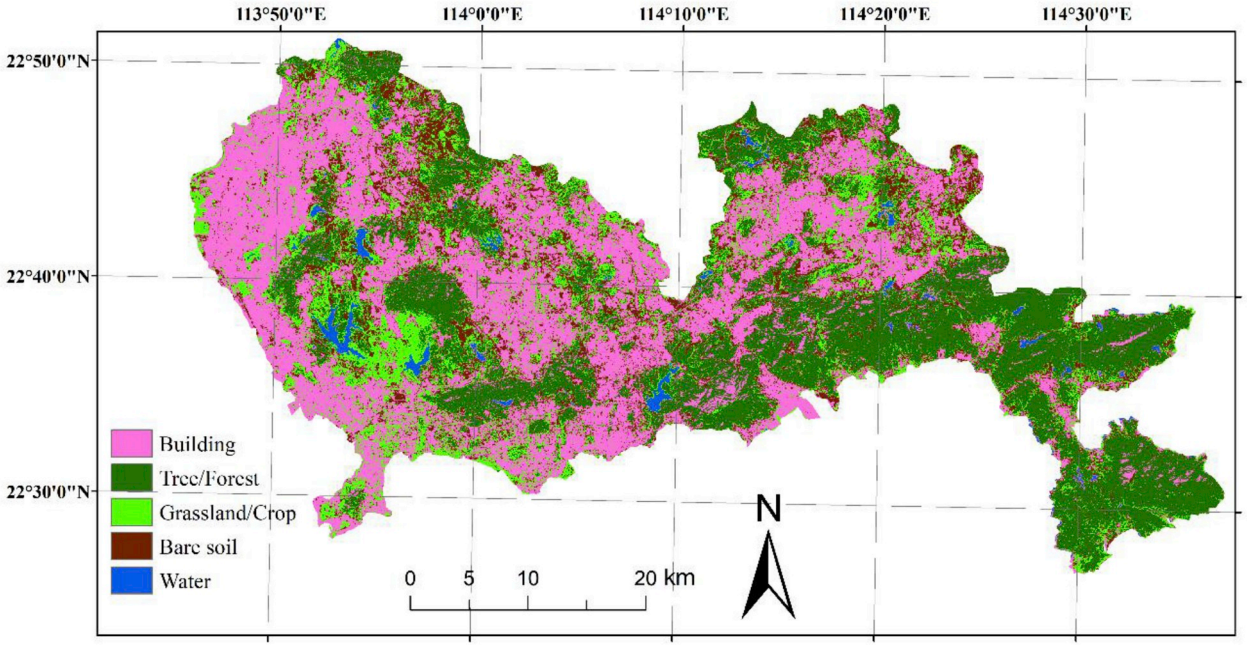

Fig. 2. Land cover classification image of Shenzhen.

(2018).

Fig. 6 and Fig. 7 exhibits the surface latent heat (LE) and sensible heat (H) results derived from the Landsat images. Among all the urban land-cover types, the thermal environmental effect of urban vegetation is significantly different from that of the other types. Based on the composition of land types, the urban vegetation mainly consists of a large amount of wood, farmland and grassland. The results also show that the thermal components are significantly different between urban built-up areas and vegetation, especially in the spatial distribution of LE and H. We can observe that the contour of the built-up area of Shenzhen is very clear, with boundaries separating the built-up area and suburban area. Because most of the underlying surface is composed of impervious materials, such as tar or cement, the LST and H of the urban built-up area is significantly higher than that of the suburban vegetation-covered area. It's found that the lack of vegetation transpiration leads to significantly lower evapotranspiration in the urban built-up area relative to the suburban area with vegetation coverage, thus resulting in a significant decrease in the urban LE. On the other hand, due to the lack of vegetation coverage, a significant increase in the sensible heat flux of the urban built-up area relative to the suburban area. Overall, the thermal pattern of Shenzhen is supported by other studies (Kato and Yamaguchi, 2007; Xu et al., 2008). It should be mentioned that since vegetation and impervious surfaces are typical characteristics of urban regions, quantitative analysis of the formation of these two cover types and the corresponding thermal ecological function is the focus of future studies. While previous studies, i.e. Chakraborty et al. (2015) and Li et al. (2016), have been more on the satellite-based urban thermal environment in term of the heat flux components in different region, there is no analysis regarding on Shenzhen which is one special represented coastal cities. Our work extended previous studies and give a meaningful reference for the studying of costal city in Asian-Pacific region.

To more comprehensively analyze the effects of land coverage on the urban thermal environments, this study further checks the statistical information of thermal components for different land coverage. Table 1 shows the average and standard deviation of the LST and heat fluxes corresponding to different land cover types. Table 2 shows the average and standard deviation of the LST and LE corresponding to different

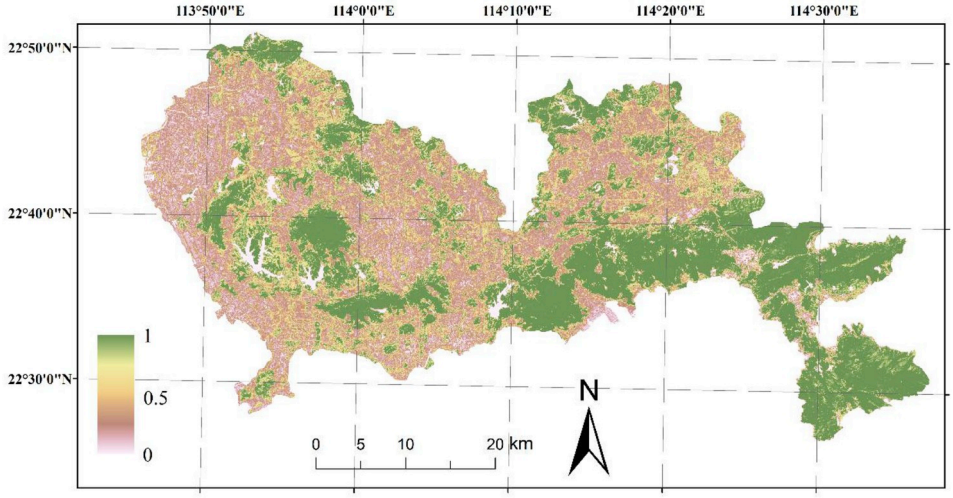

Fig. 3. Vegetation fractional coverage image of Shenzhen.

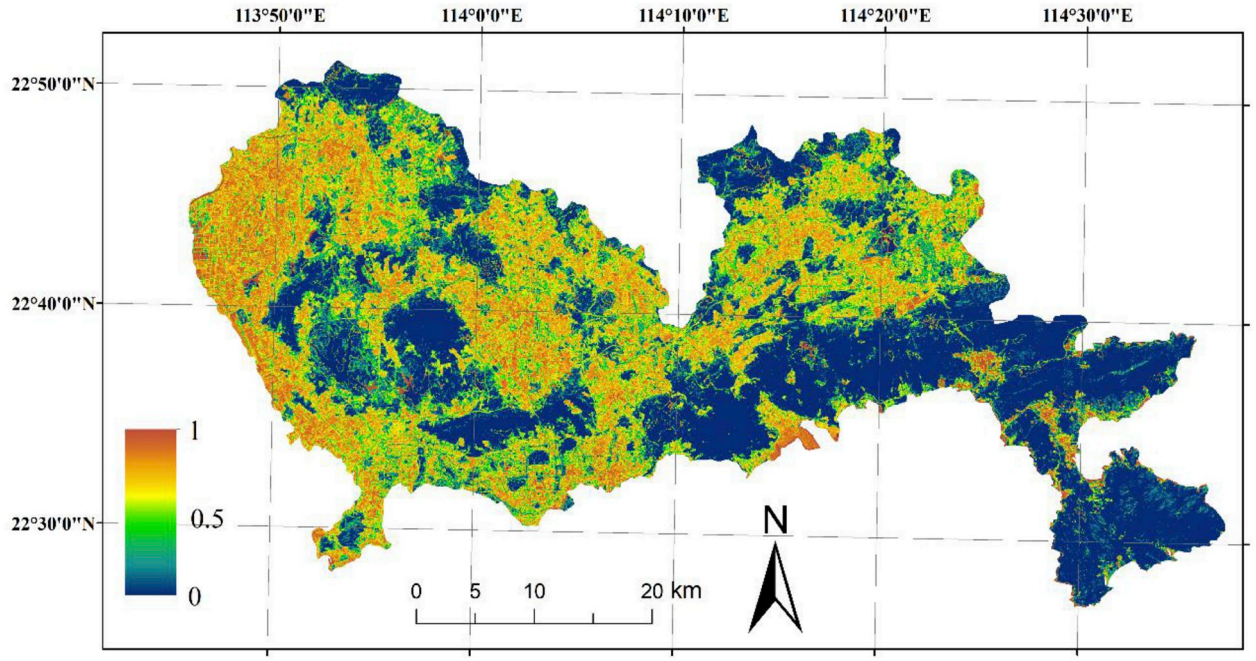

Fig. 4. Impervious surface percentage image of Shenzhen.

vegetation coverage. Table 3 shows the average and standard deviation of LST and H corresponding to different impervious surfaces coverage.

The heat balance principle demonstrates that vegetation possesses large LE, whereas buildings possess small LE and only account for a small portion of the land surface net radiation. Under the effects of solar radiation, the numerous heat-absorbing and heat-accumulation surfaces, such as cement pavement and buildings, present higher sensible heat fluxes than green land, equivalent to 15–30% of the land surface net radiation, whereas in areas with vegetation coverage, the sensible heat flux is only equivalent to 5–15% of the land surface net radiation. This finding shows that the distribution of urban vegetation coverage can greatly impact the development of the urban thermal environment (Onishi et al., 2010; Zhou et al., 2014). Therefore, studying the quantitative relationship between urban thermal environments and vegetation coverage is of great practical importance.

The urban thermal environment is subject to the combined changes of each urban interior element, and its formation mechanism is very complex. One of the most significant characteristics of the urban heat island is the significant urban-suburban temperature difference. The expansion of urban built-up areas is one of the most direct and ultimate reasons for the expansion of the urban heat island range. The fact is that, in recent decades, Shenzhen has experienced rapid urbanization and developed from a small rural town to a modern international city (WANG et al., 2009). In addition, artificial measures have changed the thermal radiation and heat accumulation pattern, which is the most significant factor for reducing the intensity of thermal environments in

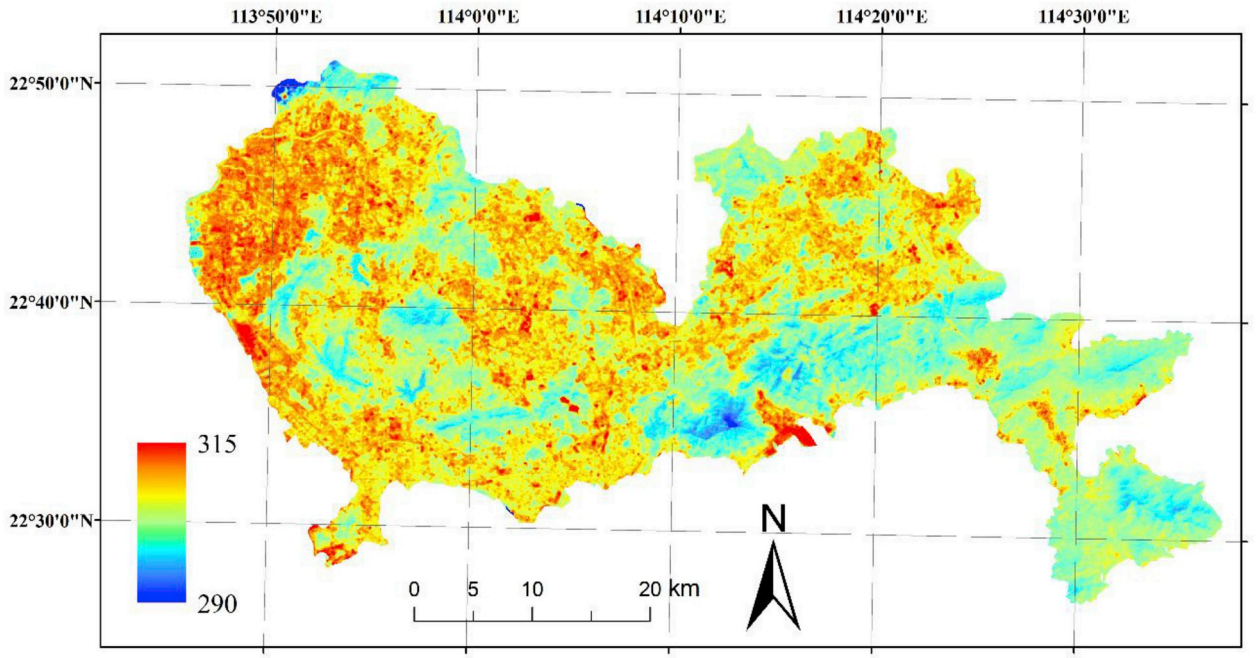

Fig. 5. Land surface temperature (in K) image of Shenzhen.

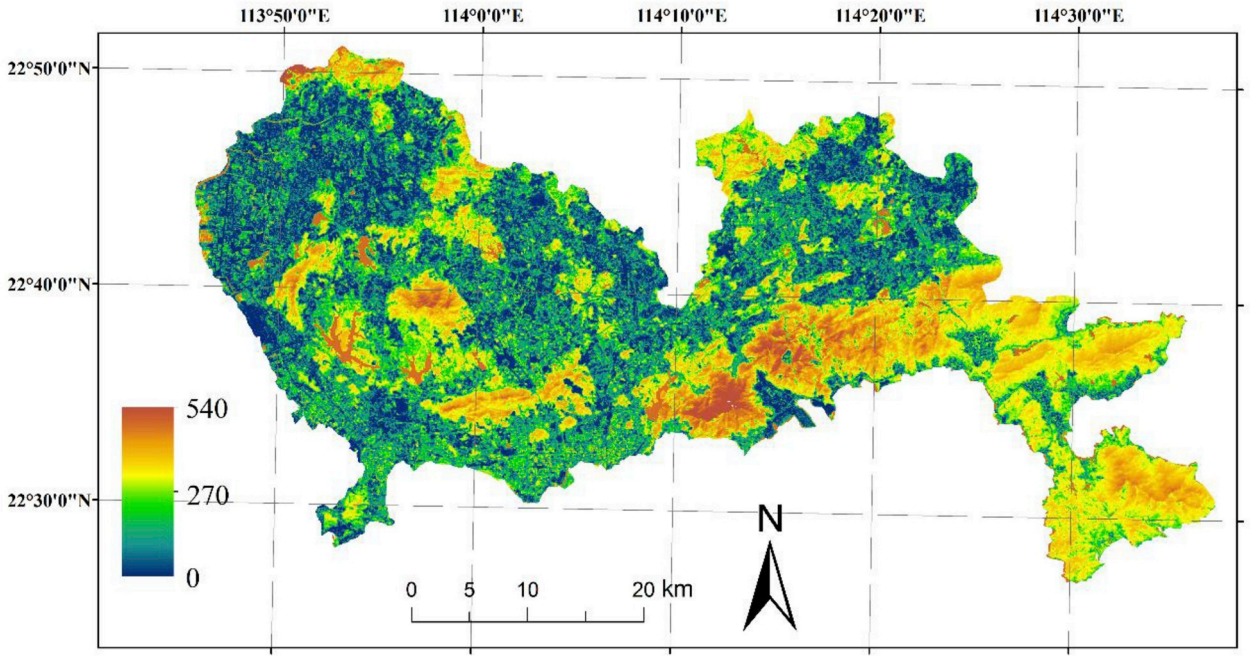

Fig. 6. Latent heat flux (in Wm^{-2}) image of Shenzhen.

Shenzhen. As a compacted city that only owns the land area of 2000 km^2 and has to sustain tens of millions people, how to solve the issues related to the urban landscapes is significant. This study helps to better understand the effect of land coverage patterns on the urban thermal environment and can provide basic research support for the optimization of urban landscapes and alleviation of the urban heat island effect.

4.2. Regulatory function of vegetation on urban heat dissipation

Since one of the research focuses is the contribution of urban vegetation to heat dissipation of land surfaces, this study attempts to analyze the relationship between the heat dissipation capacity per land

Table 1
Statistical information of different land covers (Mean: mean value, Sd: standard deviation).

Land cover types	Rn (Wm^{-2})		H (Wm^{-2})		LE (Wm^{-2})		LST (K)	
	Mean	Sd	Mean	Sd	Mean	Sd	Mean	Sd
Water	593.5	18.5	−8.9	7.6	477.3	29.2	295.6	2.1
Bare soil	490.2	35.6	17.8	8.6	157.1	31.4	302.5	2.4
Crop/Grassland	528.8	28.1	21.1	23.8	352.2	72.3	299.8	1.8
Tree/Forest	534.2	19.2	13.2	19.5	462.6	46.9	298.8	1.2
Low-dense building	491.5	24.2	90.4	36.7	207.9	85.7	302.6	2.5
High-dense building	485.7	46.4	104.9	40.2	47.8	72.7	303.3	2.9

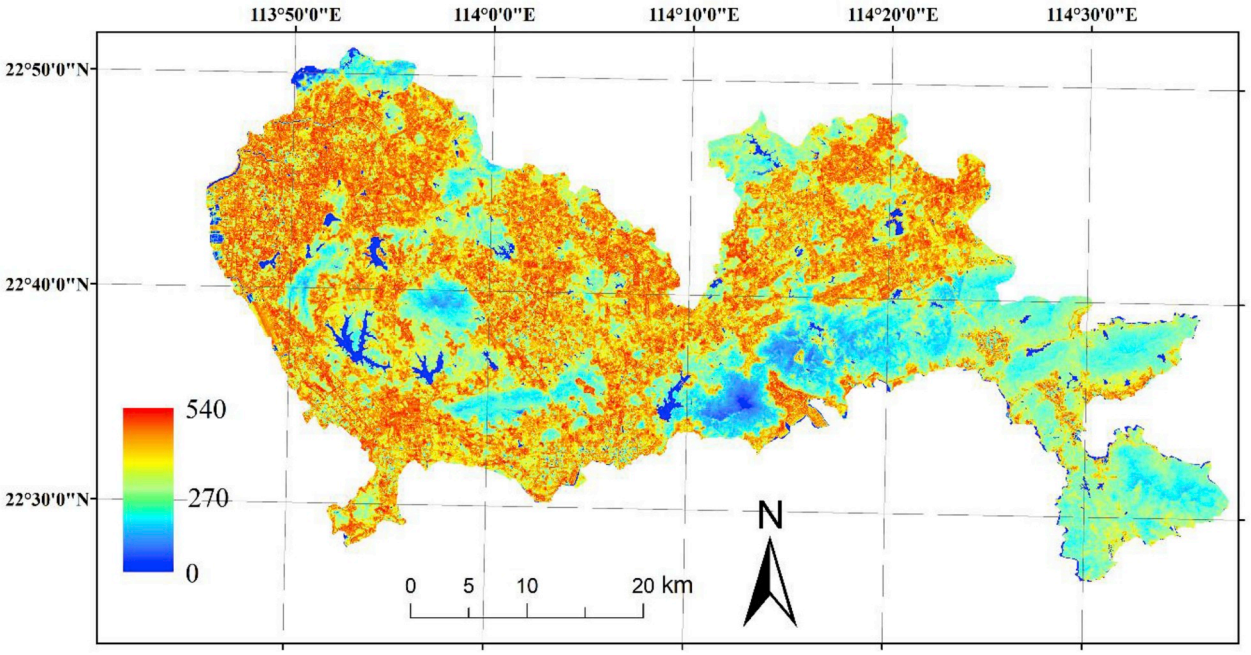

Fig. 7. Sensible heat flux (in Wm^{-2}) image of Shenzhen.

Table 2
Statistical information of different vegetation fractional covers (Mean: mean value, Sd: standard deviation).

Vegetation%	LE (Wm^{-2})		LST (K)	
	Mean	Sd	Mean	Sd
< 10%	66.5	122.8	302.6	2.7
10%–30%	174.2	122.1	302.6	2.1
30%–50%	253.3	109.7	302.5	2.3
50%–70%	325.3	98.6	301.3	2.3
> 70%	361.3	81.7	299.9	2.1

Table 3
Statistical information of different impervious surface percentage covers (Mean: mean value, Sd: standard deviation).

ISA%	H (Wm^{-2})		LST (K)	
	Mean	Sd	Mean	Sd
< 10%	15.8	23.1	299.4	1.9
10%–30%	44.2	40.1	300.9	2.3
30%–50%	61.1	46.0	301.8	2.2
50%–70%	68.0	49.6	302.8	2.1
> 70%	88.1	48.9	303.0	2.2

surface unit area (LE/FVC (vegetation fraction coverage)). Unlike some previous studies that investigate the linear correlation between vegetation parameters and LST (Mallick et al., 2013; Yuan and Bauer, 2007; Zhang et al., 2009), we focused on the non-linear correlation based on the urban heat fluxes. The pattern in the study area shows that the LE/FVC decreases drastically as the FVC increases, as shown in Fig. 8(a). The results show that areas with very small urban green land coverage (FVC < 4–8%) usually present a stronger heat dissipation capacity per unit area, which suggests that small urban green land patches in dense building areas could generate substantial latent heat, which can more effectively alleviate urban thermal radiation. This phenomenon may be related to the advective phenomenon formed by tall buildings and water bodies. Similar conclusions have been reported by relevant studies (Kuang et al., 2015; Oke, 1979; Yong-Hong et al., 2015; Zhao et al., 2014), which suggest that green land in dense urban areas possesses a higher capacity for generating latent heat.

The use of the LE/FVC to FVC ratio to analyze the urban heat dissipation capacity in this study is similar to the approach used by (Kuang et al., 2015). Other studies have also focused on these tasks from the aspect of the local LE. To ensure that evaluations of urban heat changes are repeatable and feasible for different models and different urban scenes, additional detailed analysis methods should be introduced. A reliable regional analysis method can also be used to support the above conclusions, in which the average change of LE/FVC with each 1% increase of FVC is analyzed. Similar to the above study, we also find that the average LE/FVC and FVC depict a strong statistical relationship (Fig. 8(b)), which further demonstrates that urban green land may present a strong capacity for reducing the urban heat via LE in low coverage areas. When attempting to adjust the urban heat effect, city managers should pay more attention to areas with little urban green coverage (approximately 4–8%), particularly in dense commercial areas.

5. Conclusions

Based on the Landsat 8 image of Shenzhen, this study uses a linear spectral mixture model to extract abundance information of land cover and analyzes the effects of urban land coverage on the LST and heat budget status. Two conclusions have been reached. (1) Shenzhen exhibit the urban heat island phenomenon in summer, and the LST difference among different land covers is significant. Variances in the LE and H of different urban land cover types are significant. These differences play an important role in the formation and elimination of urban heat islands. (2) In Shenzhen, the LE/FVC decreases as the FVC increases, which suggests that the relative LE generation capacity varies with the FVC. In areas with low urban green land coverage (FVC < 4–8%), a unit area of green land can generate substantial latent heat, and in dense urban areas, small patches of green land could more effectively alleviate urban heat radiation.

While one two-source urban heat flux model was found of acceptable performances in some references (Liu et al., 2017a; Weng et al., 2014), the availability of this model in Shenzhen region needs to be further assessed with some local experimental sites. This study only used one scene to analyze the urban heat island effect, more scenes that stretch on different seasons should be considered in the next step. Due to the limitation of satellite data available, meter-scale thermal satellite image has to be used for our work. Nevertheless, some effective neighborhood scale satellite data that was collected from airborne source or retrieved with the thermal fusion model should be used in the future work.

Acknowledgment

This work was supported by the National Natural Science Foundation of China (Grant No. 41671362, 41671354) and the National Natural Science Foundation of China (Grant No. 41671368, 41571175), and the special foundation for Young scientists of Zhejiang

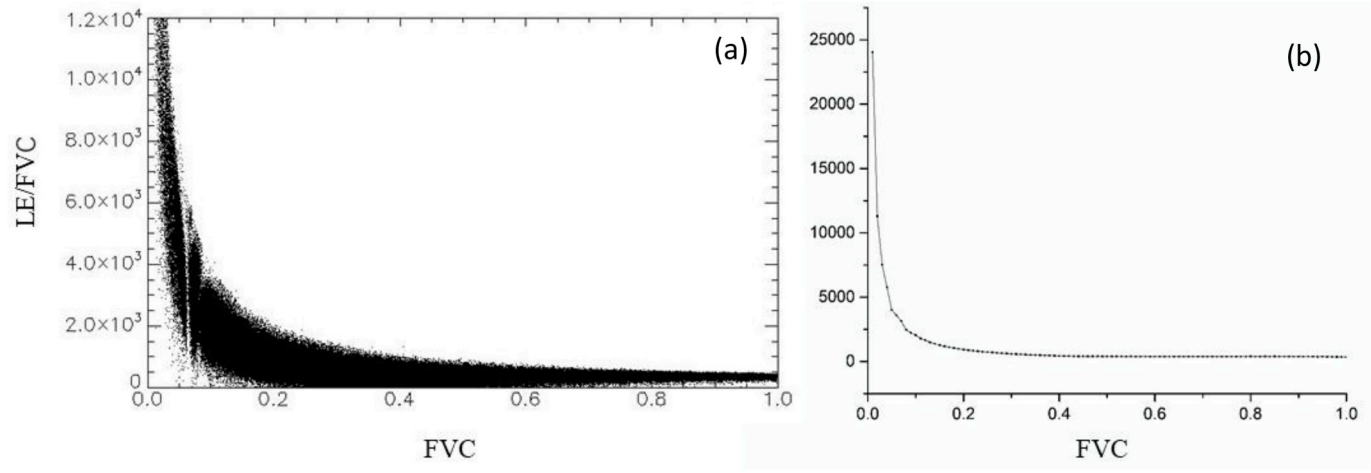

Fig. 8. Urban vegetation heat flux regulatory function based on (a) the whole image scene and (b) the average interval.

Province (Grant No. LQ18D010004). We greatly thank the State Environmental Protection Scientific Observation and Research Station for Ecology and Environment in Rapid Urbanization Region for providing the dataset.

References

Arnfield, A.J., 2003. Two decades of urban climate research: a review of turbulence, exchanges of energy and water, and the urban heat island. Int. J. Climatol. 23, 1–26.

Buyantuyev, A., Wu, J., 2010. Urban heat islands and landscape heterogeneity: linking spatiotemporal variations in surface temperatures to land-cover and socioeconomic patterns. Landsc. Ecol. 25, 17–33.

Chakraborty, S.D., Kant, Y., Mitra, D., 2015. Assessment of land surface temperature and heat fluxes over Delhi using remote sensing data. J. Environ. Manag. 148, 143–152.

Chen, X.-L., Zhao, H.-M., Li, P.-X., Yin, Z.-Y., 2006. Remote sensing image-based analysis of the relationship between urban heat island and land use/cover changes. Rem. Sens. Environ. 104, 133–146.

Chen, Z., Gong, C., Wu, J., Yu, S., 2012. The influence of socioeconomic and topographic factors on nocturnal urban heat islands: a case study in Shenzhen, China. Int. J. Rem. Sens. 33, 3834–3849.

Dennison, P.E., Roberts, D.A., 2003. Endmember selection for multiple endmember spectral mixture analysis using endmember average RMSE. Rem. Sens. Environ. 87, 123–135.

Grimmond, S., 2007. Urbanization and global environmental change: local effects of urban warming. Geogr. J. 173, 83–88.

Imhoff, M.L., Zhang, P., Wolfe, R.E., Bounoua, L., 2010. Remote sensing of the urban heat island effect across biomes in the continental USA. Rem. Sens. Environ. 114, 504–513.

Kato, S., Yamaguchi, Y., 2005. Analysis of urban heat-island effect using ASTER and ETM + Data: separation of anthropogenic heat discharge and natural heat radiation from sensible heat flux. Rem. Sens. Environ. 99, 44–54.

Kato, S., Yamaguchi, Y., 2007. Estimation of storage heat flux in an urban area using ASTER data. Rem. Sens. Environ. 110, 1–17.

Kuang, W., Dou, Y., Zhang, C., Chi, W., Liu, A., Liu, Y., Zhang, R., Liu, J., 2015. Quantifying the heat flux regulation of metropolitan land use/land cover components by coupling remote sensing modeling with in situ measurement. J. Geophys. Res.: Atmospheres 120, 113–130.

Li, X., Mitra, C., Dong, L., Yang, Q., 2018. Understanding land use change impacts on microclimate using Weather Research and Forecasting (WRF) model. Phys. Chem. Earth 103 (Parts A/B/C), 115–126.

Li, X., Wu, T., Liu, K., Li, Y., Zhang, L., 2016. Evaluation of the Chinese fine spatial resolution hyperspectral satellite TianGong-1 in urban land-cover classification. Rem. Sens. 8, 438.

Liu, K., Su, H., Li, X., 2017a. Comparative assessment of two vegetation fractional cover estimating methods and their impacts on modeling urban latent heat flux using Landsat imagery. Rem. Sens. 9, 455.

Liu, K., Zhang, X., Li, X., Jiang, H., 2014. Multiscale Analysis of Urban Thermal Characteristics: Case Study of Shijiazhuang, China. SPIE. pp. 16.

Liu, Y., Peng, J., Wang, Y., 2017b. Diversification of land surface temperature change under urban landscape renewal: a case study in the main city of shenzhen, China. Rem. Sens. 9, 919.

Liu, K., Su, H., Li, X., Wang, W., Yang, L., Liang, H., 2016. Quantifying Spatial–Temporal Pattern of Urban Heat Island in Beijing: An Improved Assessment Using Land Surface Temperature (LST) Time Series Observations From LANDSAT, MODIS, and Chinese New Satellite GaoFen-1. IEEE J. Selected Topics Appl. Earth Observat. 9, 2028–2042.

Liu, K., Su, H., Zhang, L., Yang, H., Zhang, R., Li, X., 2015. Analysis of the Urban Heat Island Effect in Shijiazhuang, China Using Satellite and Airborne Data. Rem. Sens. 7, 4804.

Mallick, J., Rahman, A., Singh, C.K., 2013. Modeling urban heat islands in heterogeneous land surface and its correlation with impervious surface area by using night-time ASTER satellite data in highly urbanizing city, Delhi-India. Adv. Space Res. 52, 639–655.

Oke, T., 1979. Advectively-assisted evapotranspiration from irrigated urban vegetation. Boundary-Layer Meteorol. 17, 167–173.

Oke, T.R., 1982. The energetic basis of the urban heat island. Q. J. R. Meteorol. Soc. 108, 1–24.

Onishi, A., Cao, X., Ito, T., Shi, F., Imura, H., 2010. Evaluating the potential for urban heat-island mitigation by greening parking lots. Urban For. Urban Green. 9, 323–332.

Otukei, J.R., Blaschke, T., 2010. Land cover change assessment using decision trees, support vector machines and maximum likelihood classification algorithms. Int. J. Appl. Earth Obs. Geoinf. 12, S27–S31.

Peng, J., Jia, J., Liu, Y., Li, H., Wu, J., 2018. Seasonal contrast of the dominant factors for spatial distribution of land surface temperature in urban areas. Rem. Sens. Environ. 215, 255–267.

Pongrácz, R., Bartholy, J., Dezső, Z., 2010. Application of remotely sensed thermal information to urban climatology of Central European cities. Phys. Chem. Earth 35 (Parts A/B/C), 95–99.

Rizwan, A.M., Dennis, L.Y.C., Liu, C., 2008. A review on the generation, determination and mitigation of Urban Heat Island. J. Environ. Sci. 20, 120–128.

Schwarz, N., Lautenbach, S., Seppelt, R., 2011. Exploring indicators for quantifying surface urban heat islands of European cities with MODIS land surface temperatures. Rem. Sens. Environ. 115, 3175–3186.

Sobrino, J.A., Jiménez-Muñoz, J.C., Paolini, L., 2004. Land surface temperature retrieval from LANDSAT TM 5. Rem. Sens. Environ. 90, 434–440.

Sobrino, J.A., Jimenez-Munoz, J.C., Soria, G., Romaguera, M., Guanter, L., Moreno, J., Plaza, A., Martinez, P., 2008. Land surface emissivity retrieval from different VNIR and TIR sensors. IEEE Trans. Geosci. Rem. Sens. 46, 316–327.

Tran, H., Uchihama, D., Ochi, S., Yasuoka, Y., 2006. Assessment with satellite data of the urban heat island effects in Asian mega cities. Int. J. Appl. Earth Obs. Geoinf. 8, 34–48.

Voogt, J.A., Oke, T.R., 2003. Thermal remote sensing of urban climates. Rem. Sens. Environ. 86, 370–384.

WANG, Y.P., WANG, Y., WU, J., 2009. Urbanization and informal development in China: urban villages in shenzhen. Int. J. Urban Reg. Res. 33, 957–973.

Weng, Q., 2009. Thermal infrared remote sensing for urban climate and environmental studies: methods, applications, and trends. ISPRS J. Photogrammetry Remote Sens. 64, 335–344.

Weng, Q., Hu, X., Quattrochi, D.A., Liu, H., 2014. Assessing Intra-Urban Surface Energy Fluxes Using Remotely Sensed ASTER Imagery and Routine Meteorological Data: A Case Study in Indianapolis, U.S.A. IEEE J. Selected Topics Appl. Earth Observat. Remote Sens. 7, 4046–4057.

Weng, Q., Lu, D., 2008. A sub-pixel analysis of urbanization effect on land surface temperature and its interplay with impervious surface and vegetation coverage in Indianapolis, United States. Int. J. Appl. Earth Obs. Geoinf. 10, 68–83.

Weng, Q., Lu, D., Schubring, J., 2004. Estimation of land surface temperature–vegetation abundance relationship for urban heat island studies. Rem. Sens. Environ. 89, 467–548.

Xu, W., Wooster, M.J., Grimmond, C.S.B., 2008. Modelling of urban sensible heat flux at multiple spatial scales: a demonstration using airborne hyperspectral imagery of Shanghai and a temperature–emissivity separation approach. Rem. Sens. Environ. 112, 3493–4351.

Yong-Hong, L., Wu-Peng, D., Xiao-Jun, X., Bing, D., 2015. A climatic environmental performance assessment method for ecological city construction: Application to Beijing Yanqi Lake. Adv. Clim. Change Res. 6, 23–25.

Yuan, F., Bauer, M.E., 2007. Comparison of impervious surface area and normalized difference vegetation index as indicators of surface urban heat island effects in Landsat imagery. Rem. Sens. Environ. 106, 375–386.

Zhang, Y., Odeh, I.O.A., Han, C., 2009. Bi-temporal characterization of land surface temperature in relation to impervious surface area, NDVI and NDBI, using a sub-pixel image analysis. Int. J. Appl. Earth Obs. Geoinf. 11, 256–264.

Zhao, L., Lee, X., Smith, R.B., Oleson, K., 2014. Strong contributions of local background climate to urban heat islands. Nature 511, 216–219.

Zhou, W., Qian, Y., Li, X., Li, W., Han, L., 2014. Relationships between land cover and the surface urban heat island: seasonal variability and effects of spatial and thematic resolution of land cover data on predicting land surface temperatures. Landsc. Ecol. 29, 153–167.